Sorting Circulating Tumor Cells: A Low Flow Microfluidic Pre-Enrichment Function for Improved Separation in Serial Two-Stage Sorting Device

Emma Dupont[1,2] [a], Emilie Laffont[1,2], Marie Piecyk[3] [b], Léa Payen[3] [c], Clément Albin[2],
Gilles Simon[2], Damien Le Roy[2] [d] and Anne-Laure Deman[1] [e]

[1]*Université Claude Bernard Lyon 1, CNRS, INSA Lyon, Ecole Centrale de Lyon, CPE Lyon, INL, UMR5270 69621 Villeurbanne, France*
[2]*Université Claude Bernard Lyon 1, CNRS, Institut Lumière Matière, UMR5306, F-69100, Villeurbanne, France*
[3]*Laboratoire de Biochimie Et Biologie Moléculaire, Groupe Hospitalier Sud, Hospices Civils de Lyon, 69495 Pierre Bénite, France*

Keywords: Cell Separation, Circulating Tumor Cells, Dean Vortices, Liquid Biopsy, Micro Milling, Microfluidic Device, Passive Separation, Size Sorting, Spiral Microchannel.

Abstract: The isolation of Circulating Tumor Cells (CTCs) directly from blood by liquid biopsy could lead to a paradigm shift in clinical cancer care by enabling earlier diagnosis, more accurate prognosis and personalized treatment. Nevertheless, the specific challenges of CTCs, including their rarity and heterogeneity, have so far limited the use of CTCs in clinical studies. Currently, no device fully meets the requirements of high recovery, high purity, short processing time and ease of use for end-users. A promising new strategy involves combining a higher throughput but less specific pre-enrichment step based on size sorting together with a highly specific but slower immunomagnetic sorting. This approach requires the initial function to operate at lower flow rates than commonly used to connect the two functions in series. In this context, we developed a Dean spiral microfluidic device, optimized for sorting 10μm and 15μm beads by size. We showed that it successfully separates mimicking CTCs from white blood cells at low flow rates (<100 mL/h).

1 INTRODUCTION

Circulating tumor cells (CTCs) have been biomarkers of interest to the medical community for many years. Originating from the patient tumor and accessible by blood sampling, they can be used to enhance our understanding of metastasis dynamics, improve cancer detection (through liquid biopsy) (Mazzitelli, et al., 2023), prognosis assessment and refine monitoring strategies (CellSearch, 2024). Despite the appealing interests of CTCs, a major issue stands in the way of their recovery. The CTC are extremely rare in the blood: 1-1000 CTC per mL, i.e. 1-1000 CTC per 10^7 white blood cells (WBC) and 10^9 red blood cells (RBC) (Stoecklein, et al., 2016), making the sorting complex. Moreover, CTC sorting must fulfill some requirements. First, it must have a high recovery rate (>90%): the fraction of CTCs being very low in a blood sample, it is necessary to get the maximum of them downstream of the process. Secondly, the purity of the sample is also crucial. The other blood cells are outnumbered compared to the CTCs, and they may pollute the downstream analysis, so the purity of the sorting must be high (>99,99%). Additionally, it is important to preserve cell viability during isolation.

Studies in the literature generally isolate CTCs from other blood cells based on differences in their biological or physical properties, such as surface

[a] https://orcid.org/0009-0007-8381-3080
[b] https://orcid.org/0009-0000-3765-9472
[c] https://orcid.org/0000-0002-1599-5886
[d] https://orcid.org/0000-0002-3111-6044
[e] https://orcid.org/0000-0001-9351-8703

marker expression or size, deformability, and dielectric properties. In terms of biological properties, two strategies are possible: positive enrichment by labelling CTCs with magnetic nanoparticles or negative depletion by labelling WBCs. However, not all CTCs express the same markers on their surface, so there is a risk of losing some of them by targeting a specific marker. Furthermore, labelling WBCs with anti-CD15 or anti-CD45 markers is not fully efficient, and some WBCs remain non-magnetic. The biological approach has therefore its limitations. Alternatively, physical property differences can be exploited to separate CTCs from other blood cells by driving them into different outlets. This method offers high throughput without any labelling steps, but if the physical properties are too similar, a precise separation is challenging. For instance, CTCs are typically larger than WBCs and RBCs (Hou et al., 2013). However, the overlapping size range between CTCs and WBCs inevitably limits the purity of the isolation process.

Much work has been published in the literature in recent years on sorting CTCs in microsystems (Qiao, et al., 2024) (Descamps, et al., 2022), and devices have been commercialized (Parsortix PC1, ANGLE, Genesis System, BIORAD; ClearCell FX1, BIOLIDICS; VTX-1 Liquid Biopsy System, VORTEX) but CTC analysis is still not routinely carried out in hospitals. Indeed, despite significant successes, isolation methods relying on a single separation technique do not meet all the CTC sorting requirements mentioned earlier. A promising approach is to combine two different sorting methods to make up for the shortcomings of each, using physical separation method as a pre-enrichment step followed by an immunomagnetic sorting step (Li, et al., 2024) (Nian, et al., 2024) (Descamps, et al., 2021).

Combining two functions in microfluidics is challenging as each function optimally operates at a different flow rate. In particular, hydrodynamic devices often work at much higher flow rates than immunomagnetic ones. In this work we set out to develop a hydrodynamic pre-enrichment function operating at low flow rates. Dean vortices have been widely studied as a size-based CTC sorting technique, using inertial microfluidics to position particles within the channel based on their size. Different systems have been developed yielding promising results (Zhu, et al., 2024) (Akbarnataj, et al., 2023) (Al-Halhouli, et al., 2018) at flow rates ranging from 100-300mL/h. Here we report on a design of Dean flow device that operates at lower flow rates (<100 mL/h) compared to most spirals developed for CTC

sorting, and that can be used as a pre-enrichment step prior to an immunomagnetic sorting step.

2 DEVICE FABRICATION

2.1 Microchannel Design

In rectangular straight microchannels, the equilibrium position of a particle, in the section of the channel of width w and height h, is mainly due to lift forces (Di Carlo, et al., 2009):

$$F_L = \frac{\rho U^2 a_p^4}{D_h^2} f_L (Re, x_p) \ (N) \qquad (1)$$

where ρ is the fluid density, U the fluid mean velocity (m/s), a_p the particle diameter, and $D_h = wh/(w + h)$ is the hydraulic diameter of the channel and f_L a lift coefficient ranged between 0.02-0.05, depending on Re the Reynolds number and x_p, the particle position in the channel.

In curved channels, the curvature creates a pressure gradient in the channel, which leads to the formation of two counter-rotating vortices, known as Dean vortices. In such vortices, a particle is submitted to the Dean drag force, which can be expressed as (Di Carlo, et al., 2007):

$$F_D = \rho \frac{U^2 a_p D_h^2}{R} \ (N) \qquad (2)$$

where R is the radius curvature of the spiral. The Dean number De is often use to quantitively characterize the strength of secondary flows in such channels:

$$De = Re \sqrt{\frac{D_h}{2R}} \qquad (3)$$

The higher it is, the stronger are the secondary vortices. A particle flowing in a spiral or curved channel is then mainly subjected to F_L and F_D in the section perpendicular to the main flow. The competition between these two forces is often used to describe the particle behavior and predict its equilibrium positions in the channel section. It is important, for particle size sorting, to note that both forces depend on the particle diameter a_p ($F_D \sim a_p$ and $F_L \sim a_p^4$). This results in two distinct behaviors: bigger particles tend to focus at an equilibrium position and remain in a specific location within the channel's section, while smaller particles tend to be dragged into Dean's vortices and recirculate across

the channel width (Bhagat A. A., et al., 2010), (Wu, et al., 2012).

To effectively separate WBCs from CTCs in a spiral microfluidic channel, we aim to focus the two populations in separate locations of the channel width. We have designed a spiral channel based on key principles described in the literature.

First, to ensure proper particle focusing, we considered the confinement ratio of the particle. As outlined by Di Carlo et al. (2007), this ratio must satisfy:

$$\frac{a_p}{D_h} > 0.07 \tag{4}$$

to achieve proper focusing. Another critical parameter is the ratio of lift forces to Dean forces, as described by Amini et al. (2014). They established the inequality:

$$R_f = \frac{F_L}{F_D} \sim \frac{2Ra_p^2}{D_h^3} > \sim 0.08 \tag{5}$$

This inequality, derived from their previous experimental results and other study (Di Carlo, et al., 2007), provides a guideline for selecting suitable spiral geometry to achieve efficient particle focusing.

Secondly, a trapezoidal cross-section was selected to enhance size-based separation across the channel. This design introduces asymmetry in the flow profile, which shifts the Dean vortices centres toward the outer wall of the channel. As a result, smaller particles, such as WBCs, entrained in the vortices, are pushed toward the outer wall, whereas larger particles, like CTCs, remain focused near the inner wall. This configuration significantly improves the separation efficiency between different size populations. (Wu, et al., 2012) (Akbarnataj, et al., 2023).

In order to operate at lower flow rates, we developed a spiral with a reduced cross-sectional area compared to those reported in the literature. The reduction in channel dimensions aims to achieve the necessary velocities to generate Dean vortices at low flow rates.

Based on these criteria, we designed a 6-loops spiral with one inlet and two outlets, an internal radius of 1 mm and a trapezoidal cross-section. The width w of the channel is 250 μm, the height of the inner wall of the channel is 60 μm and the height of the outer one is 85 μm. The spacing between the windings is equal to the width of the micro-channels.

2.2 Microsystem Fabrication Steps

To create a microchannel with a trapezoidal cross-section, a mold with variable height was required.

The master mold was fabricated by micro-milling (CNC Mini-Mill/3, Minitech Machinery Corporation) on brass (Figure 1.A.1) in a two-step process (Figure 1.B). First the horizontal contour of the spiral has been milled using 500 μm and 200 μm flat nose end mill. Secondly, the machining of the top wall of the channel (which is inclined due to the trapezoidal cross-section) was obtained using a 200 μm diameter ball nose mill with z-axis steps of 1 μm. A SEM-image and the profile (Dektak150, Veeco) of the channel are shown in Figure 1.C and Figure 1.D. The microchannels were then fabricated by casting PDMS (Sylgard Silicone Elastomer, 10:1 base and curing agent mixing ratio) on the mold and curing it at 65°C during 2 h (Figure 1.A.2). After curing, the PDMS was peeled from the mold and plasma bonded to a 1 mm thick flat glass slide to complete the microchannel (Figure 1.A.5). Input and output ports of 0.5 mm were punched prior to bonding step with the Uni-Core TM Puncher. Figure 1.E shows a picture of the PDMS final device.

3 MATERIALS AND METHODS

3.1 Sample Preparation

For bead experiments, fluorescent-polystyrene particles with diameter of 10 μm (9.9 ± 0.09 μm, blue), 15 μm (15.4 ± 0.139 μm, red) (Thermofisher scientific), were diluted in Phosphate-buffered saline (PBS). A solution containing both bead populations was prepared with equal concentrations of 1.10^6 beads/mL for each population.

For cells and blood sample experiments, MDA-MB-231 and MCF7 cells were cultured to mimic the CTC in blood. The cells were stained with Hoechst (1μL/mL, blue) for 15 minutes at 37°C, followed by three centrifugation (1000 rpm, 5 minutes) and resuspension (in 1xPBS) steps. The final concentration used was 9.10^6 cells/mL (MDA) and 10.10^6 cells/mL (MCF7). All experiments involving healthy blood samples were carried out in conformity with the relevant French laws and institutional guidelines and approved by the French national blood collection institution, named "Etablissement Français du Sang" (EFS). All healthy volunteers gave informed consent for the collection of blood samples. Blood samples were collected from healthy volunteers into EDTA tubes (BD Vacutainer). Red blood cells were first removed using a lysis buffer x 1 (EurX®, E0326-02). Following the manufacturer's protocol, lysis buffer was added in a 1 : 4 v/v ratio (blood/lysis buffer) and incubated for 10 min at room

temperature (RT) and then centrifuged at $500 \times g$ for 10 min. After centrifugation, the supernatant, containing lysed red blood cells, is discarded. The WBCs, contained in the pellet, are stained with Hoechst (1 µL/mL, blue) following the same steps as for the MDA and MCF7 cells. The WBCs are counted in Malassez cells at around 9.10^6 cells/mL. The behaviors of the cell populations in the device were characterized independently.
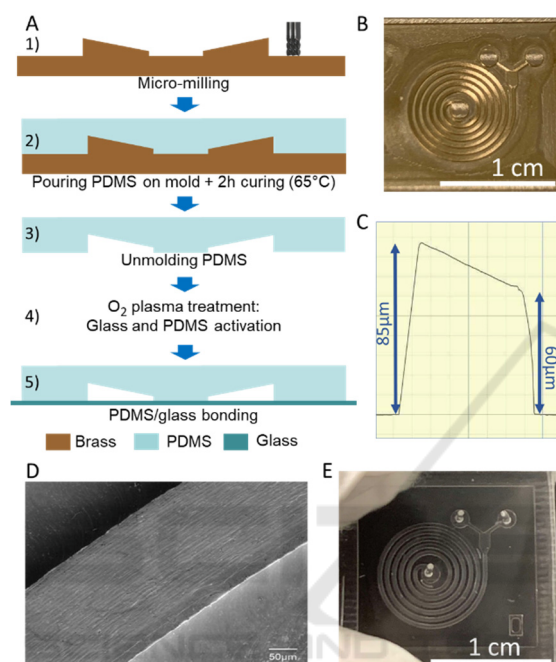

Figure 1: A) Device fabrication steps. 1) Micro-milling of the brass mold, 2) Pouring and curing of PDMS 3) Unmolding PDMS and 4) O₂ plasma treatment 5) bonding on glass slide B) Picture of the brass mold C) 2D-Profil of the spiral channel cross-section. The vertical distortion is due to the stylus tip angle D) SEM picture of a 6th turn portion and E) Picture of the final device in PDMS.

3.2 Acquisition Method

The different sample solutions have been injected in the spiral channel with a syringe pump (DKInfusetek, ISPLab02). Fluorescents images were recorded with Thunder microscope (Leica Microsystems). The fluorescence signal intensities for each bead populations were extracted with ImageJ and subsequently processed on MATLAB. On the boxplots (Figure 2.B and Figure 4), the central mark indicates the median value, and the bottom and top edges of the box indicate the 25th and 75th percentiles of the intensity throughout the channel width, respectively. The whiskers extend to the most extreme data points not considered outliers.

4 RESULTS AND DISCUSSION

4.1 Microbeads Separation

In this section, we aimed to separate the 10 µm and 15 µm bead populations into distinct, narrow streams across the channel width. The following sections focus on identifying the optimal conditions for effective separation. To achieve that, we investigated the bead trajectories at flow rates ranging from 10 to 120 mL/h.

4.1.1 Flow Rate Dependency of Bead Positioning

Images of the spiral outlet were taken, just before the bifurcation into two separate outlets, at various flow rates, as depicted in Figure 2.A. Depending on the flow rate, the beads were observed to focus into either a single stream or two closely spaced streams.

When examining the focusing positions across the channel width, both bead populations demonstrated similar migration patterns (Figure 2.B), as reported in the literature (Martel, et al. 2013) (Guan, et al., 2013). At low flow rates (10–20 mL/h), the two bead populations remained mixed and focused near the channel center. As the flow rate increased, both populations began migrating toward the inner wall of the channel, but at different flow rates: the small 10 µm beads reached their most inner position at around 30 mL/h, while the large 15 µm beads reached this position at higher flow rate, at around 60 mL/h. The location of the inner equilibrium position also differs between the two populations, with the larger beads focusing closer to the inner wall than the smaller ones. At even higher flow rates, both bead populations migrated toward the outer wall of the channel. This outward migration occurred at lower flow rates for the 10 µm beads compared to the 15 µm ones. By 120 mL/h, both populations have moved to a similar position close the outer wall of the channel. As suggested in the literature, this position may correspond to the center of the Dean vortices (Wu, et al., 2012).

Additionally, one can notice that at flowrate in which the beads move through the channel section (i.e. are not in a specific equilibrium position), the observed focusing beam may widen or split into two adjoining sub-beams.
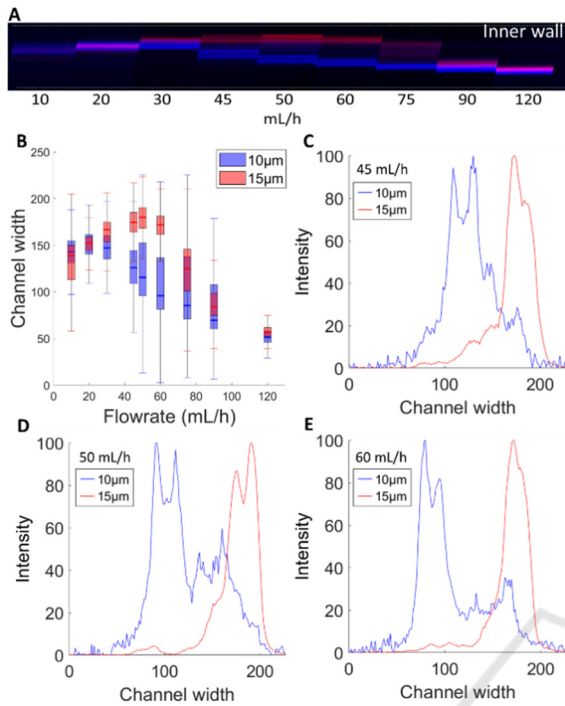
Figure 2: A) Superimposed images of the 10 µm (blue) and 15 µm (red) beads flowing through the last turn of the spiral. B) Boxplot of the fluorescence intensity repartition in the channel width, 0 µm being the outer wall and 250 µm the inner one. C-E) Fluorescence intensity signal of the two beads populations at the outlet at 45, 50 and 60 mL/h.

Since the transition of bead positions occurs at different flow rates, we can identify the flow rates at which the 10µm beads are positioned near the outer wall, while the 15 µm beads remain near the inner wall, allowing for separation. The bead streams are separated at three flow rates: 45 mL/h, 50 mL/h and 60 mL/h. The corresponding florescent signals for these flow rates are shown in figure 2.C-E. Most beads in each population concentrate into a single stream. However, some of them remain slightly unfocused, and must be considered when determining the optimal flow rate for separation.

The flow rate of 60 mL/h provides the best separation, offering the largest gap between the two populations while minimizing overlap caused by unfocused beads.

4.1.2 Beads Focusing Along the Spiral

Beside flowrate analysis, the focusing of the beads has also been investigated in the different turns of the spiral. In the literature, the number of turns of the spiral varies from 1 to 12 depending on the spiral design. Amini et al (Amini, Wonhee, & Di Carlo,

2014) expressed the length L required for particles to reach their equilibrium positions:

$$L = f \frac{\pi \mu h^2}{\rho U_m a^2 f_l} \quad (m) \qquad (6)$$

where U_m the fluid max velocity in the channel (m/s). To account for the shorter particle focusing distance at high De values (typically De>17), the authors introduces f, a scaling factor ranged from 0.2 to 1, depending on the curving channel design, with a value of 1 applied for lower De. For our design, at 60 mL/h, $De = 25$. Using $f = 0.2$ and according to (6), the minimum distance for the 10 µm and 15 µm beads to focus is 9 mm and 4 mm respectively. According to our spiral dimensions, both populations should be focused after the 2nd turn (
Table 1).

Table 1: Length of the spiral at each turn.

Turn	1	2	3	4	5	6
Length (mm)	4.3	13.7	26.3	42.0	60.9	82.9

Experimentally, the beads gradually focus into their equilibrium position as they move through the turns (Figure 3A). By the second turn, the 15 µm beads are already tightly focused into a single stream, whereas the 10 µm beads remain in a larger stream (Figure 3B).
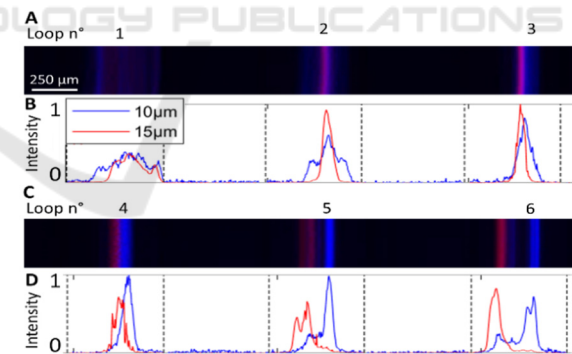

Figure 3: A-C) Picture of the beads solution flowing throughout the turns at 60 mL/h. B-D) 10 µm (blue) and 15 µm (red) fluorescence intensity in the spiral turns from the first one (left) to the 6th and last one (right).

As the beads move along the curved microchannel, the positions of the two populations progressively move apart, with one (15 µm) focusing along the inner side of the channel and the other along the opposite side, reaching maximum separation in the final turn.

4.2 Device Performances on WBC and Mimicking CTC

To mimic the behavior of CTCs in a microfluidic spiral channel and investigate their separation from WBCs, we characterized the behavior of MDA-MB-231 cancer cells (average diameter 12-14 μm), MCF7 cancer cells (average diameter 18μm) commonly used in the literature to mimic CTC (Macaraniag, et al., 2023). We also circulated WBCs, whose sizes vary significantly depending on their type, with an average diameter ranging from 7 to 12 (Hou et al., 2013), at flow rates ranging from 10 to 120 mL/h.

We first analyzed the lateral focusing and position of these cells at the outlet, as shown in Figure 4. Even if cells are deformable and vary in size (i.e., non-monodisperse), all three cell types focused into distinct single streams at the channel outlet across all tested flow rates.

In terms of equilibrium positions within the channel, all the cell types exhibited a behavior similar to the one observed with beads. As the flow rate increased, the cells initially migrated toward an equilibrium position near the inner wall of the channel and, at higher flow rates, they gradually shifted toward the outer wall.

Interestingly, each cell type exhibited this migration at different flow rates, correlating with their size. WCBs reached their innermost equilibrium position at a relatively low flow rate of around 20 mL/h, the slightly larger MDA-MB-231 cells reached this position at approximately 45 mL/h, and the largest ones, MCF7, focus near the inner wall at even higher flow rates, around 60 mL/h. Notably, MDA-MB-231 cells focused closer to the inner wall than WBCs, consistent with the bead study findings based on their size. While size-dependent behavior suggests MCF7 cells would focus closer to the inner wall than MDA, their inner position remained farther away, likely due to the channel's spatial constraints (65 μm height in this region). Additionally, it was observed that the MDA cells focused in wider streams than the other two cell populations.

Our results illustrate a clear size-dependent behavior: smaller cells migrate toward the inner wall at lower flow rates compared to larger cells, enabling effective size-based cell separation. To separate WBCs and MDA-MB-231 cells, the optimal flow rate for maximum separation is 50 mL/h. The interquartile distance between the two focused streams is then approximately 22,5 μm, which is sufficient to direct them into separate outlets at the channel exit.
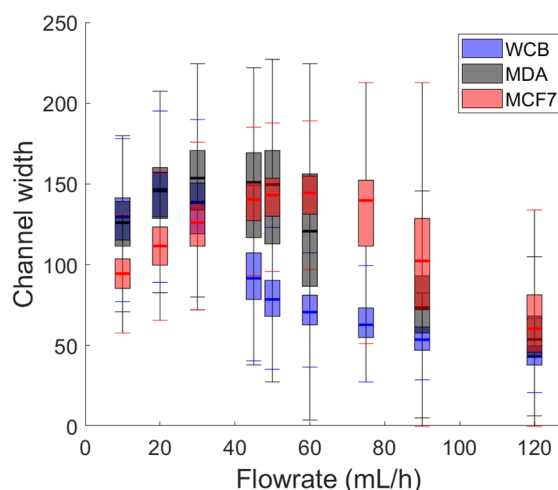

Figure 4: Boxplot of the fluorescence intensity repartition of 3 cell populations in the channel width.

This separation is even more pronounced at 60 mL/h between WBCs and MCF7 cells, given their larger size difference. At this flow rate, MCF7 cells remain at their innermost position, while WBCs have already migrated outward, maintaining a 50 μm interquartile distance. Although MCF7 cells are commonly used to mimic CTCs due to their large size, it is essential to consider both MCF7 and MDA-MB-231 populations during sorting to best represent the size diversity of the CTCs.

This size-dependent equilibrium positioning enables the collection of different cell types based on their distinct stream locations, ensuring efficient separation of larger CTCs from smaller WBCs. This isolation can be achieved with our spiral between 50 and 75mL/h, at lower flowrates than spirals in the literature (Zhu, et al., 2024) (Akbarnataj, et al., 2023) (Al-Halhouli, et al., 2018).

5 CONCLUSIONS

In a context of growing interest for CTC, the combination, via a serial connection, of two microfluidic functions (a pre-enrichment and a sorting one) appears to be an efficient CTC sorting strategy. This integrated approach necessitates that the initial microfluidic system operates at low flow rates (<100 mL/h), enabling it to function coherently with the other microfluidic function. Our findings demonstrate the successful development of a Dean spiral microfluidic device that efficiently separates particles depending on their size, in particular 10 μm and 15 μm beads, at low flow rates. It is also effective in sorting WBCs from mimicking CTCs in a range of

optimum flow rates of 50-75 mL/h. This sorting function not only demonstrates efficient separation but also operates at flow rates that are easily compatible with immunomagnetic sorting. These promising results suggest that this approach can be effectively integrated with additional microfluidic functions, to achieve high-purity, high-recovery CTC sorting.

ACKNOWLEDGEMENTS

REFERENCES

Akbarnataj, K., Maleki, S., Rezaeian, M., Haki, M., & Shamloo, A. (2023). Novel size-based design of spiral microfluidic devices with elliptic configurations and trapezoidal cross-section for ultra-fast isolation of circulating tumor cells. *Talenta*.

Al-Halhouli, A., Al-Faqheri, W., Alhamarneh, B., Hecht, L., & Dietzel, A. (2018). Spiral microchannels with trapezoidal cross section fabricated by femtosecond laser ablation in glass for the inertial separation of microparticles. *Micromachines, 9*(4).

Amini, H., Wonhee, L., & Di Carlo, D. (2014). Inertial microfluidic physics. *Lab on a Chip, 14*(15).

Bhagat, A. A., Kuntaegowdanahalli, S. S., & Papautsky, I. (2008). Continuous particle separation in spiral microchannels using dean flows and differential migration. *Lab Chip, 8*, 1906–1914.

Bhagat, A. A., Kuntaegowdanahalli, S. S., Kaval, N., Seliskar, C. J., Papautsky, I., & e. (2010). Inertial microfluidics for sheath-less high-throughput flow cytometry. *Biomedical Microdevices, 12*, 187-195.

Castro-Giner, F., & Aceto, N. (2020). Tracking cancer progression: from. *Genome Medicine, 12*(1).

CellSearch Circulating Tumor Cell. (2024, January 10). *Clinical application*. (Menarini Silicon Biosystems, Inc) Retrieved from https://www.cellsearchctc.com/clinical-applications/mbc-clinical-trials-case-studies

Descamps, L., Le Roy, D., & Deman, A. L. (2022). Microfluidic-Based Technologies for CTC Isolation: A Review of 10 Years of Intense Efforts towards Liquid Biopsy. *International Journal of Molecular Sciences*.

Descamps, L., Marie-Charlotte, A., Jordyn, H., Samir, M., Clément, A., David, B., . . . Deman, A.-L. (2021). Self-Assembled Permanent Micro-Magnets in a Polymer-Based. *Cells*.

Di Carlo, D. (2009). Inertial microfluidics. *Lab on a Chip, 9*(21).

Di Carlo, D., Irimia, D., Tompkins, R. G., & Toner, M. (2007). Continuous inertial focusing, ordering, and separation. *PNAS, 104*(48), 18892–18897.

Gao, W., Yuan, H., Jing, F., Wu, S., Zhou, H., Mao, H., . . . Jia, C. (2017). Analysis of circulating tumor cells from lung cancer patients with multiple biomarkers using high-performance size-based microfluidic chip. *Oncotarget, 8*, 12917-12928.

Guofeng Guan, Lidan Wu, Ali Asgar S. Bhagat, Zirui Li, Peter C. Y. Chen, Shuzhe Chao, Chong Jin Ong & Jongyoon Han. (2013). Spiral microchannel with rectangular and trapezoidal cross-sections for size based particle separation. *Scientific Reports, 3*, 1475.

Hou, H. W., Warkiani, M. E., Khoo, B. L., Li, Z. R., A, R., Tan, D. S.-W., . . . Lim, C. T. (2013). Isolation and retrieval of circulating tumor. *Scientific Reports, 3*.

Joseph M. Martel and Mehmet Toner. (2013). Particle focusing in curved microfluidic channels. *Scientific Reports, 3*.

Krawczyk, N., Meier-Stiegen, F., Banys, M., Neubauer, H., Ruckhaeberle, E., & Fehm, T. (2014). Expression of Stem Cell and Epithelial-Mesenchymal TransitionMarkers in Circulating Tumor Cells of Breast Cancer Patients. *BioMed Research International*.

Li, Q., Wang, Y., Gao, W., Qian, G., Chen, X., & Liu, Y. S. (2024). A microfluidic device for enhanced capture and high activity release of heterogeneous CTCs from whole blood. *Talanta*.

Macaraniag, C., Zhou, J., Li, J., Putzbach, W., Hay, N., & Papautsky, I. (2023). Microfluidic isolation of breast cancer circulating tumor. *Electrophoresis*, 1859-1867.

Man Lee, L., Klarmann, G. J., Haithcock, D. W., Wang, Y., Bhatt, H., Prabhakarpandian, B., . . . Lai, E. (2023). Label-free Enrichment of Human Adipose-Derived Stem Cells using a Continuous Microfluidic Sorting Cascade. *Lab on Chip*.

Mazzitelli, C., Santini, D., Gianluca Corradini, A., Zamagni, C., Trerè, D., Montanaro, L., & Taffurelli, M. (2023). Liquid Biopsy in the Management of Breast Cancer Patients: Where Are We Now and Where Are We Going. *Diagnostics, 13*, 1241.

Nian, M., Chen, B., He, M., & Hu, B. (2024). A Cascaded Phase-Transfer Microfluidic Chip with Magnetic Probe for High-Activity Sorting, Purification, Release, and Detection of Circulating Tumor Cells. *Analytical Chemistry*.

Nikolas H., S., Fischer, J. C., Niederacher, D., & Terstappen, L. W. (2016). Challenges for CTC-based liquid biopsies: Low CTC frequency and diagnostic

leukapheresis as a potential solution. *Expert Review of Molecular Diagnostics, 16*(2), 147-164.

Qiao, Z., Xiangyu, T., Anqin, L., & Wenguang, Y. (2024). Novel Isolating Approaches to Circulating Tumor Cell. *Micromachines*.

Wu, L., Guan, G., Hou, H. W., Bhagat, A. A., & Han, J. (2012). Separation of Leukocytes from Blood Using Spiral Channel with. *American Chemical Society*, 9324-9331.

Xiang, N., Wang, J., Li, Q., Han, Y., Huang, D., & Ni, Z. (2019). Precise Size-Based Cell Separation via the Coupling of Inertial Microfluidics and Deterministic Lateral Displacement. *Analytical Chemistry, 91*, 10328-10334.

Zhu, Z., Ren, H., Wu, D., Ni, Z., & Xiang, N. (2024). High-throughput and simultaneous inertial separation of tumor cells and clusters from malignant effusions using spiral-contraction-expansion channels. *Microsystems and Nanoengineering*.